Bioorganic Chemistry 49 (2013) 9–15

Contents lists available at SciVerse ScienceDirect

Bioorganic Chemistry

journal homepage: www.elsevier.com/locate/bioorg

Ligand-based CoMFA and CoMSIA studies on chromone derivatives as radical scavengers

Narumol Phosrithong [a], Jiraporn Ungwitayatorn [b,*]

[a] Faculty of Pharmacy, Siam University, 38 Petkasem Road, Bangkok 10160, Thailand
[b] Faculty of Pharmacy, Mahidol University, 447 Sri-Ayudhya Road, Bangkok 10400, Thailand

ARTICLE INFO

Article history:
Received 27 December 2012
Available online 12 June 2013

Keywords:
Chromone derivatives
Radical scavenging activity
CoMFA
CoMSIA

ABSTRACT

The antioxidant activity for a series of chromone compounds, evaluated by DPPH free radical scavenging assay, were subjected to 3D-QSAR studies using comparative molecular field analysis (CoMFA) and comparative molecular similarity indices analysis (CoMSIA). All 48 chromone derivatives were geometry optimized by AM1 and HF/6-31G* calculations. The CoMFA and CoMSIA results were compared between different alignment strategies. The best CoMFA model obtained from HF/6-31G* optimization with field fit alignment gave cross-validated r^2 (q^2) = 0.821, noncross-validated r^2 = 0.987, S = 0.095, and F = 388.255. The best CoMSIA model derived from AM1 optimized structures and superimposition alignment gave q^2 = 0.876, noncross-validated r^2 = 0.976, S = 0.129, and F = 208.073, including electrostatic, hydrophobic, hydrogen bond donor and acceptor fields. The contour maps provide the fruitful structure–radical scavenging activity relationships which are useful for designing new compounds with higher activity.

1. Introduction

Flavonoids are natural phenyl substituted chromones which show many biological and pharmacological activities [1] such as anti-inflammatory [2,3], anti-allergic [3], antimicrobial [2], estrogenic [2,4], anti-HIV [5,6] and anticancer activities [7,8]. Recent interests in natural antioxidants have been stimulated by potential health benefits arising from the antioxidant activity of flavonoids [9–11]. Flavonoids like many other polyphenols are very effective radical scavengers (chain-breaking antioxidants) because they are highly reactive hydrogen or electron donors [12–14]. Structure–activity relationship (SAR) studies of flavonoids have indicated the importance of the number and location of the phenolic OH groups for effective radical scavenging activity [15–17].

In the previous study, we have designed and synthesized a series of chromone derivatives and evaluated for their radical scavenging activity using 1,1-diphenyl-2-picrylhydrazyl (DPPH) free radical scavenging activity (Table 1). 7,8-Dihydroxy-2-(3′-trifluoromethylphenyl)-3-(3″-trifluoromethylbenzoyl) chromone, **32**, was found to be the most active antioxidant with the IC_{50} = 4.95 ± 0.02 μM [18]. Chromone **32** was more potent than the known antioxidant flavonoids, quercetin (IC_{50} = 10.89 μM), luteolin (IC_{50} = 11.0 μM) and fisetin (IC_{50} = 14.06 μM) [19]. To explore the relationships between the structures of these compounds and their antioxidant activity, a three-dimensional quantitative structure–activity relationship (3D-QSAR) study using comparative molecular field analysis (CoMFA) and comparative molecular similarity indices analysis (CoMSIA) were performed in this study. In the absence of information regarding the biological target, indirect ligand-based approaches 3D-QSAR such as CoMFA and CoMSIA can assist in clarifying the SARs.

CoMFA is a versatile and powerful tool in rational drug design and related applications. CoMFA samples the steric (Lennard–Jones) and electrostatic (Coulombic) fields surrounding a set of ligands and constructs a 3D-QSAR model by correlating these 3D steric and electrostatic fields with the corresponding observed activities. Partial least squares (PLS) analysis, with a cross validation procedure, is employed to select relevant components from the large set of CoMFA data to build up the best QSAR equation [20]. CoMSIA is an extension of the CoMFA methodology and differs only in the implementation of the fields [21,22]. In CoMSIA approach, hydrophobic, hydrogen bond donor and hydrogen bond acceptor similarity fields are calculated in addition to the steric and electrostatic fields, which provides a better interpretation of the correlations between the 3D structures of the studied molecules and their activities. The fields are evaluated by a PLS analysis similar to CoMFA. The obtained CoMFA and CoMSIA contour maps results are used as visual guides for design of the new and more potent radical scavenging compounds.

* Corresponding author. Fax: +66 2 644 8695.
E-mail address: jiraporn.ung@mahidol.ac.th (J. Ungwitayatorn).

0045-2068/$ - see front matter © 2013 Elsevier Inc. All rights reserved.
http://dx.doi.org/10.1016/j.bioorg.2013.06.003

Table 1
Structures and the radical scavenging activity of the studied chromone derivatives.

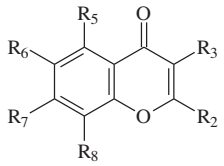

.

Compd.	R_2	R_3	R_5	R_6	R_7	R_8	IC_{50} (μM)
1	Phenyl	H	H	H	H	OH	371.78 ± 1.87
2	CH_3	H	H	H	OH	OH	17.50 ± 0.41
3	Benzyl	H	H	H	OH	OH	5.93 ± 0.07
4	Phenyl	H	H	H	OH	OH	13.62 ± 1.23
5	CH_3	H	H	H	OH	H	199.15 ± 0.97
6	Benzyl	H	H	H	OH	H	77.15 ± 0.77
7	Benzyl	CH_3	H	H	OH	H	911.92 ± 8.36
8	Phenyl	H	H	H	OH	H	1518.51 ± 11.31
9	Phenyl	CH_3	H	H	OH	H	1202.82 ± 12.16
10	4′-(NO_2)-Phenyl	H	H	H	OH	H	1103.52 ± 13.00
11	3′-(CF_3)-Phenyl	H	H	H	OH	H	381.01 ± 3.56
12	4′-(F)-Phenyl	H	H	H	OH	H	696.20 ± 3.90
13	3′,5′-(diNO_2)-Phenyl	H	H	H	OH	H	1145.89 ± 13.09
14	3′-(Cl)-Phenyl	H	H	H	OH	H	697.51 ± 9.30
15	3′,4′-(diCl)-Phenyl	H	H	H	OH	H	518.49 ± 8.30
16	4′-(*t*-butyl)-Phenyl	H	H	H	OH	H	517.12 ± 7.99
17	3′-(CF_3)-Phenyl	H	OH	H	OH	H	993.04 ± 14.11
18	4′-(F)-Phenyl	H	OH	H	OH	H	481.64 ± 6.21
19	3′,4′-(diF)-Phenyl	H	OH	H	OH	H	340.16 ± 4.49
20	4′-(*t*-butyl)-Phenyl	H	OH	H	OH	H	353.09 ± 5.74
21	4́-(NO_2)-Phenyl	H	OH	H	OH	H	491.74 ± 8.04
22	3′,5′-(diNO_2)-Phenyl	H	OH	H	OH	H	409.66 ± 2.29
23	3′-(Cl)-Phenyl	H	OH	H	OH	H	550.50 ± 7.73
24	3′,4′-(diCl)-Phenyl	H	OH	H	OH	H	742.82 ± 10.75
25	4′-(OCH_3)-Phenyl	H	OH	H	OH	H	516.47 ± 516.47
26	3′-(OCH_3)-Phenyl	H	OH	H	OH	H	678.67 ± 28.26
27	3′-(OCH_3)-Phenyl	H	H	OH	H	H	1106.21 ± 4.59
28	3′-(Cl)-Phenyl	H	H	OH	H	H	1112.54 ± 27.15
29	4′-(F)-Phenyl	H	H	OH	H	H	981.07 ± 11.36
30	3′-(CF_3)-Phenyl	H	H	OH	H	H	935.71 ± 26.59
31	4′-(*t*-butyl)-Phenyl	H	H	OH	H	H	2476.91 ± 24.63
32	3′-(CF_3)-Phenyl	3″-(CF_3)-benzoyl	H	H	OH	OH	4.95 ± 0.02
33	3′-(Cl)-Phenyl	3″-(Cl)-benzoyl	H	H	OH	OH	11.82 ± 0.04
34	3′-(OCH_3)-Phenyl	3″-(OCH_3)-benzoyl	H	H	OH	OH	10.24 ± 0.15
35	4′-(F)-Phenyl	4″-(F)-benzoyl	H	H	OH	OH	13.95 ± 0.03
36	4′-(NO_2)-Phenyl	4″-(NO_2)-benzoyl	H	H	OH	OH	11.49 ± 0.17
37	4′-(OCH_3)-Phenyl	4″-(OCH_3)-benzoyl	H	H	OH	OH	12.15 ± 0.07
38	3′,4′-(diF)-Phenyl	3″,4″-(diF)-benzoyl	H	H	OH	H	553.95 ± 1.70
39	3′-(CF_3)-Phenyl	3″-(CF_3)-benzoyl	H	H	OH	H	405.32 ± 4.45
40	3′-(Cl)-Phenyl	3″-(Cl)-benzoyl	H	H	OH	H	523.11 ± 4.42
41	3′-(OCH_3)-Phenyl	3″-(OCH_3)-benzoyl	H	H	OH	H	597.11 ± 0.85
42	4′-(F)-Phenyl	4″-(F)-benzoyl	H	H	OH	H	572.53 ± 5.42
43	4′-(NO_2)-Phenyl	4″-(NO_2)-benzoyl	H	H	OH	H	362.25 ± 6.26
44	4′-(OCH_3)-Phenyl	4″-(OCH_3)-benzoyl	H	H	OH	H	559.49 ± 4.68
45	4′-(*t*-butyl)-Phenyl	4″-(*t*-butyl)-benzoyl	H	H	OH	H	408.18 ± 4.97
46	3′-(OCH_3)-Phenyl	3″-(OCH_3)-benzoyl	OH	H	OH	H	531.59 ± 4.28
47	4′-(NO_2)-Phenyl	4″-(NO_2)-benzoyl	OH	H	OH	H	353.40 ± 11.37
48	4′-(*t*-butyl)-Phenyl	4″-(*t*-butyl)-benzoyl	H	OH	H	H	1217.90 ± 27.79

2. Materials and methods

2.1. Biological activity data of chromone derivatives

The radical scavenging activity of chromone derivatives was determined by DPPH assay [18]. The IC_{50} values (μM) from DPPH assay (Table 1) were expressed as pIC_{50} ($-\log IC_{50}$). The total of 48 molecules was divided into a training set and a test set (38 molecules in training set and 10 molecules in the test set). The training and test set compounds were chosen manually such that low, moderate, and high activity compounds were present in approximately equal proportions in both sets. The test set was used to evaluate the predictive power of the CoMFA and CoMSIA models.

2.2. Generating the 3D structures

The 3D structures of all studied compounds were modeled with SYBYL 8.1 molecular modeling program (Tripos Associates, Saint Louis, MO) on Indigo Elan workstation (Silicon Graphics Inc., Mountain View, CA) using sketch approach. The fragment libraries in SYBYL database containing of small molecules were used as building blocks for the construction of larger ones. Each structure was first energy minimized using the standard Tripos force field with a distance-dependent dielectric function and the Powell conjugate gradient algorithm. Convergence criteria of 0.01 kcal/(mol Å) was used for energy minimization. The partial atomic charges were calculated using the Gasteiger–Hückel method.

Table 2
CoMFA result (grid space 2.0 Å, column filtering 2.0 kcal/mol and energy cut off 30.0 kcal/mol).

		AM1		HF/6-31G*
		Superimposition	Field fit	Field fit
Cross-validation	Optimal components	6	5	6
	q^2	0.817	0.671	0.821
	S	0.356	0.469	0.352
Non-cross validation	r^2	0.949	0.958	0.987
	S	0.188	0.167	0.095
	F	95.809	147.199	388.255
Contribution	Steric	0.468	0.431	0.450
	Electrostatic	0.532	0.569	0.550

2.3. Geometry optimization

The minimized structures were geometry optimized by semi-empirical AM1 using MOPAC 6.0 or by *ab initio* HF/6-31G* using Gaussian 03W program package. The fully geometrical optimized structures were used in the following 3D QSAR studies.

2.4. Structural alignment

Structural alignment is the most crucial step in the CoMFA study. The AM1 optimized molecules were aligned by superimposition and field fit functions in SYBYL 8.1 and the HF/6-31G* optimized structures were aligned by field fit function.

The superimposition of molecules was based on trying to minimize root-mean-squares (rms) differences in the fitting of selected

Table 3
The experimental, calculated activities, and the residuals of CoMFA.

Compd.	pIC_{50}						
	Experimental	AM1				HF/6-31G*	
		Superimposition		Field fit		Field fit	
		Calculated	Residual	Calculated	Residual	Calculated	Residual
Training set							
1	3.429	4.017	−0.588	3.854	−0.425	3.649	−0.220
2	4.761	5.030	−0.269	4.819	−0.058	4.687	0.074
3	5.226	5.229	−0.003	5.218	0.008	5.220	0.006
4	4.868	4.586	0.282	4.663	0.205	4.668	0.200
6	4.110	4.022	0.088	3.833	0.277	4.043	0.067
7	3.040	3.142	−0.102	3.155	−0.115	3.014	0.026
9	2.919	2.806	0.113	2.993	−0.075	2.941	−0.023
11	3.420	3.553	−0.133	3.348	0.072	3.404	0.016
12	3.157	3.250	−0.093	3.255	−0.098	3.211	−0.054
13	2.942	3.067	−0.125	2.974	−0.032	3.046	−0.104
14	3.156	3.120	0.036	3.209	−0.053	3.247	−0.091
15	3.286	3.166	0.120	3.273	0.013	3.266	0.020
16	3.288	3.281	0.006	3.246	0.041	3.321	−0.034
18	3.318	3.453	−0.135	3.335	−0.017	3.182	0.136
19	3.465	3.398	0.067	3.374	0.091	3.464	0.001
20	3.451	3.393	0.058	3.526	−0.075	3.457	−0.006
21	3.310	3.324	−0.014	3.493	−0.183	3.331	−0.021
22	3.388	3.182	0.206	3.009	0.379	3.443	−0.055
23	3.260	3.310	−0.050	3.501	−0.241	3.270	−0.010
24	3.128	3.287	−0.160	3.242	−0.115	3.201	−0.074
25	3.288	3.231	0.057	3.266	0.022	3.364	−0.076
26	3.162	2.946	0.216	3.116	0.046	3.232	−0.070
28	2.937	2.810	0.127	2.716	0.221	2.848	0.089
29	3.005	2.668	0.337	2.764	0.241	2.963	0.042
30	3.023	2.965	0.058	3.028	−0.005	3.031	−0.008
31	2.606	2.699	−0.093	2.671	−0.065	2.491	0.115
32	5.308	5.040	0.268	5.162	0.146	5.280	0.028
33	4.927	4.842	0.085	4.822	0.105	5.005	−0.078
34	4.988	4.792	0.196	4.825	0.163	4.975	0.013
36	4.940	4.979	−0.039	5.095	−0.155	4.970	−0.030
37	4.916	4.805	0.111	4.956	−0.040	4.953	−0.037
39	3.391	3.560	−0.169	3.598	−0.207	3.494	−0.103
40	3.284	3.356	−0.072	3.405	−0.121	3.362	−0.078
42	3.243	3.250	−0.093	3.255	−0.098	3.141	0.102
43	3.442	3.500	−0.058	3.405	0.037	3.298	0.144
44	3.251	3.325	−0.074	3.358	−0.107	3.169	0.082
45	3.388	3.539	−0.152	3.317	0.070	3.255	0.133
46	3.271	3.408	−0.137	3.248	0.023	3.394	−0.123
Test set							
5	3.697	3.586	0.111	3.889	−0.192	3.359	0.338
8	2.819	3.050	−0.231	3.524	−0.705	3.267	−0.448
10	2.958	3.215	−0.257	3.413	−0.455	3.281	−0.323
17	3.004	3.659	−0.655	3.508	−0.504	3.553	−0.549
27	2.940	2.774	0.166	2.570	0.370	2.609	0.331
35	4.857	4.693	0.164	4.861	−0.004	4.866	−0.009
38	3.256	3.302	−0.046	3.385	−0.129	3.255	0.001
41	3.223	3.307	−0.084	3.535	−0.312	3.201	0.022
47	3.451	3.605	−0.154	3.633	−0.182	3.644	−0.193
48	2.918	2.964	−0.046	2.478	0.440	2.505	0.413

atoms with those of a template molecule. The most active chromone **32** was used as a template molecule. All atoms of the benzopyran-4-one nucleus were selected for superimposition. The conformations that exhibited minimum rms after superimposition procedure were selected and stored in the database for the next step.

The field fit procedure was used as another alignment criteria to increase field similarity within a series of studied molecules. The rms differences in the sum of steric and electrostatic interaction energies averaged across all (possibly weighted) lattice points, between the studied molecule and the template was minimized to find the best fit. Chromone **32** was also used as the template molecule in field fit alignment.

2.5. CoMFA and CoMSIA setup

CoMFA and CoMSIA were performed using the QSAR option in SYBYL 8.1. In CoMFA, the cubic grid space was generated around molecules in the training set based on the molecular volume of the structures. A sp^3-carbon atom was probed with a +1.0 unit charge, 2.0 Å grid spacing, and the default 30 kcal/mol energy cutoff for steric and electrostatic fields.

CoMSIA was performed using five physicochemical properties, i.e., steric, electrostatic, hydrophobic, hydrogen bond donor and hydrogen bond acceptor. These parameters were evaluated using common probe atom with 1 Å radius, charge +1.0, hydrophobicity +1.0, hydrogen bond donor and acceptor properties +1.0. Similarity indices were calculated using Gaussian-type distance dependence between the probe and the atoms of the molecules of the data set. This functional form required no arbitrary definition of cutoff limits, and similarity indices were calculated at all grid points inside and outside the molecule. The value of the attenuation factor α was set to 0.3.

PLS methodology was used for all 3D-QSAR analyses. The grid had a resolution of 2.0 Å and extended beyond the molecular dimensions by 4.0 Å in all directions. Column filtering was set to 2.0 kcal/mol. CoMFA and CoMSIA models were developed using the conventional stepwise procedure. The optimum number of components used to derive the non-validated model was defined as the number of components leading to the highest cross-validated r^2 (q^2) and the lowest standard error of prediction (SEP). The q^2 values were derived after "leave-one-out" cross-validation. The noncross-validated models were assessed by the explained variance r^2, standard error of estimate (S) and F ratio. The noncross-validated analyses were used to make predictions of pIC_{50} of the chromone derivatives from the test set and to display the coefficient contour maps. The actual versus predicted pIC_{50} were fitted by linear regression, and the "predictive" r^2, S, and F ratio were determined.

3. Results and discussions

3.1. CoMFA study

CoMFA was carried out to evaluate the steric and electrostatic properties associated with the radical scavenging activity of the studied chromone derivatives. Table 2 summarizes the statistical results of the CoMFA models from different alignment methods. The cross-validated correlation coefficient, q^2 defines the goodness of prediction whereas the conventional (noncross-validated) correlation coefficient, r^2 indicates goodness of fit of a QSAR model. The q^2 derived from the HF/6-31G* optimized structures and field fit alignment was higher than those from AM1 optimized geometry with superimposition and field fit alignments. The best CoMFA model gave $q^2 = 0.821$ with optimum number of components = 6, a noncross-validated $r^2 = 0.987$, standard error of estimation (S) = 0.095, and $F = 388.255$. The steric and electrostatic fields contributed to the QSAR equation by 45.0%, and 55.0%, respectively.

The experimental), the calculated pIC_{50} and the residuals (the differences between the experimental and the calculated values) of the predictions from the best CoMFA model are shown in Table 3. The scattered plots of the actual and predicted pIC_{50} of compounds in the training set and test set are depicted in Fig. 1a.

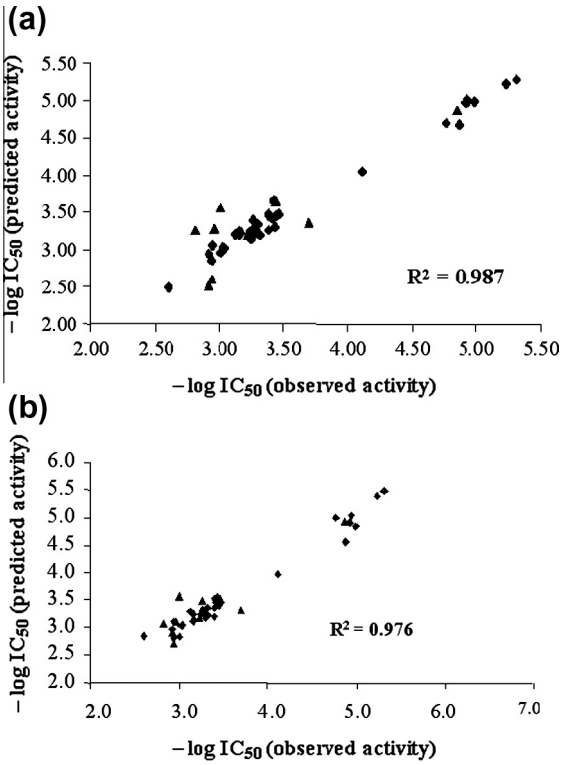

Fig. 1. Experimental versus calculated pIC_{50} for the training set (♦) and the test set (▲) (a) CoMFA model, HF/6-31G* optimization and field fit alignment. (b) CoMSIA model, AM1 optimization and superimposition alignment.

Table 4
CoMSIA statistic results.

		AM1		HF/6-31G*
		Superimposition	Field fit	Field fit
Cross-validation	Optimal components	6	6	6
	q^2	0.876	0.775	0.670
	S	0.290	0.312	0.329
Non-cross validation	r^2	0.976	0.963	0.959
	S	0.129	0.160	0.168
	F	208.073	133.792	120.741
	Steric	–	0.151	0.406
	Electrostatic	0.295	0.533	0.594
Contributions	Hydrophobic	0.206	–	–
	H-donor	0.342	–	–
	H-acceptor	0.157	0.316	–

3.2. CoMSIA study

The CoMSIA study was performed using the same PLS protocol and stepwise procedure as in the CoMFA study. The best CoMSIA model was obtained from AM1 optimized structures with superimposition alignment criteria (Table 4). This CoMSIA model gave

q^2 = 0.876 with optimum number of component = 6, a noncross-validated r^2 = 0.976, S = 0.129, and F = 208.073, including electrostatic, hydrophobic, hydrogen bond donor and acceptor fields. In this model, electrostatic, hydrophobic, hydrogen bond donor, and hydrogen bond acceptor fields contributed to the QSAR equation by 29.5%, 20.6%, 34.2%, and 15.7%, respectively. The experimental, calculated pIC_{50}, and the residuals of the predictions are shown in Table 5. The scattered plots of the actual and predicted pIC_{50} of compounds in the training set and test set from the best CoMSIA model are illustrated in Fig. 1b. The statistical outcomes and the linearity of the scattered plots indicate the high fitting and predictive abilities of both CoMFA and CoMSIA models.

3.3. CoMFA and CoMSIA contour maps

The QSARs produced by CoMFA and CoMSIA models are usually represented as 3D coefficient contour maps and these contour maps are useful for exploring SARs. Fig. 2a and b illustrate the CoMFA contour maps from the HF/6-31G* optimization and field fit alignment. The molecular structure of chromone **32** was displayed inside the field as the reference structure. The green contours represent the regions of favorable steric substituents, and yellow contours represent regions of disfavorable steric substituents. As shown in Fig. 2a, the steric group is preferred at C-8. Electronegative substituent (the red contours) should be located

Table 5
The experimental, calculated activities, and the residuals of CoMSIA.

Compd.	PIC_{50}						
	Experimental	AM1				HF/6-31G*	
		Superimposition		Field fit		Field fit	
		Calculated	Residual	Calculated	Residual	Calculated	Residual
Training set							
1	3.429	3.557	−0.128	3.797	−0.368	3.940	−0.511
2	4.761	4.985	−0.224	4.819	−0.058	4.771	−0.010
3	5.226	5.389	−0.163	5.411	−0.185	5.171	0.055
4	4.868	4.561	0.307	4.764	0.104	4.645	0.223
6	4.110	3.960	0.150	3.723	0.387	4.122	−0.012
7	3.040	3.058	−0.018	3.026	0.014	3.017	0.023
9	2.919	2.957	−0.039	2.887	0.031	3.002	−0.083
11	3.420	3.458	−0.038	3.373	0.047	3.421	−0.001
12	3.157	3.246	−0.089	3.183	−0.026	3.341	−0.184
13	2.942	3.112	−0.170	3.146	−0.204	3.012	−0.070
14	3.156	3.121	0.035	3.145	0.011	3.144	0.012
15	3.286	3.173	0.113	3.159	0.127	3.313	−0.027
16	3.288	3.270	0.017	3.147	0.140	3.432	−0.145
18	3.318	3.363	−0.045	3.416	−0.098	3.046	0.272
19	3.465	3.456	0.009	3.410	0.055	3.375	0.090
20	3.451	3.444	0.007	3.453	−0.002	3.462	−0.011
21	3.310	3.222	0.088	3.185	0.125	3.295	0.015
22	3.388	3.212	0.176	3.334	0.054	3.310	0.078
23	3.260	3.303	−0.043	3.402	−0.142	3.293	−0.033
24	3.128	3.283	−0.156	3.335	−0.208	3.153	−0.026
25	3.288	3.223	0.065	3.418	−0.130	3.393	−0.105
26	3.162	3.146	0.016	3.120	0.042	3.277	−0.115
28	2.937	2.818	0.119	2.858	0.079	2.657	0.280
29	3.005	2.826	0.179	2.760	0.245	2.898	0.107
30	3.023	3.033	−0.010	3.079	−0.056	3.062	−0.039
31	2.606	2.847	−0.241	2.605	0.001	2.567	0.039
32	5.308	5.485	−0.177	5.203	0.105	5.218	0.090
33	4.927	4.917	0.010	4.826	0.101	4.893	0.034
34	4.988	4.836	0.152	4.727	0.261	4.828	0.160
36	4.940	5.037	−0.097	4.933	0.007	4.755	0.185
37	4.916	4.911	0.005	4.936	−0.020	5.082	−0.166
39	3.391	3.539	−0.148	3.666	−0.275	3.723	−0.332
40	3.284	3.266	0.018	3.266	0.018	3.471	−0.187
42	3.243	3.246	−0.089	3.183	−0.026	3.229	0.014
43	3.442	3.391	0.051	3.385	0.057	3.321	0.121
44	3.251	3.262	−0.011	3.326	−0.075	3.192	0.059
45	3.388	3.349	0.038	3.482	−0.095	3.179	0.209
46	3.271	3.297	−0.026	3.376	−0.105	3.378	−0.107
Test set							
5	3.697	3.340	0.357	3.636	0.061	3.686	0.011
8	2.819	3.073	−0.254	3.200	−0.381	3.577	−0.758
10	2.958	3.115	−0.157	3.074	−0.116	3.386	−0.428
17	3.004	3.565	−0.561	3.577	−0.573	3.468	−0.464
27	2.940	2.719	0.221	2.563	0.377	2.536	0.404
35	4.857	4.930	−0.073	4.866	−0.009	4.683	0.174
38	3.256	3.485	−0.229	3.485	−0.229	3.307	−0.051
41	3.223	3.187	0.036	3.264	−0.041	3.464	−0.241
47	3.451	3.498	−0.047	3.534	−0.083	3.539	−0.088
48	2.918	2.923	−0.005	3.203	−0.285	2.326	0.592

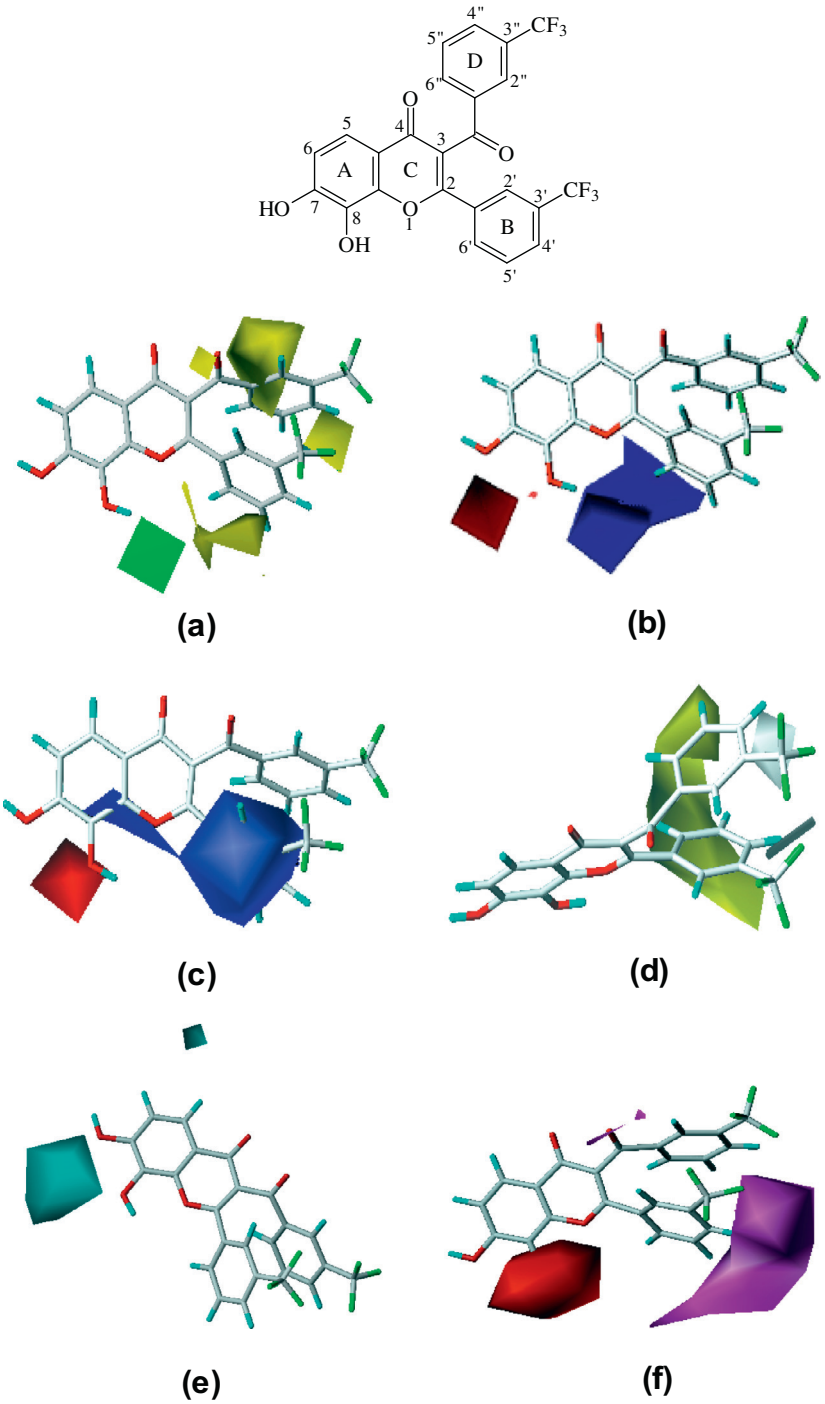

Fig. 2. CoMFA steric contour map (a) and electrostatic contour map (b). The green contour refers to sterically favored region; the yellow contours indicate disfavored areas. The blue contour indicates region where electropositive substituent is favored and red contour refers to region where electronegative substituent is favored. CoMSIA electrostatic contour map (c). CoMSIA hydrophobic contour map (d), green and white contours indicate regions where hydrophobic group favored and disfavored the activity, respectively. CoMSIA hydrogen bond donor contour map (e), cyan contours represent areas where hydrogen bond donor group favored. CoMSIA hydrogen bond acceptor contour map (f), magenta and red contours indicate regions where hydrogen bond acceptor group favored and disfavored, respectively. (For interpretation of the references to color in this figure legend, the reader is referred to the web version of this article.)

around C-7 and C-8 of ring A and electropositive substituent (the blue contours) around O-1 of ring C and C-6′ of ring B (Fig. 2b).

The contour maps of the CoMSIA model derived from AM1 optimization with superimposition alignment are shown in Fig. 2c–f. The electrostatic contour maps (Fig. 2c) were corresponding to those of CoMFA. The hydrophobic contour map (Fig. 2d) shows that the hydrophobic substituents (green contours) at C-2 and C-3 of chromone nucleus and hydrophilic group (white contours) at C-3″ and C-4″ of ring D might increase activity. The hydrogen bond donor and acceptor fields gave more contribution (49.9%) to the QSAR equation than the other fields. The hydrogen bond donor and acceptor contour maps (Fig. 2e and f) indicate that hydrogen bond donor group should be located at C-7 and C-8 and hydrogen bond acceptor group around C-3′, C-4′ and C-5′ in ring B. The underlying of the presence of OH groups at C-7 and C-8 leading to increased activity could be explained by the ease of H atom

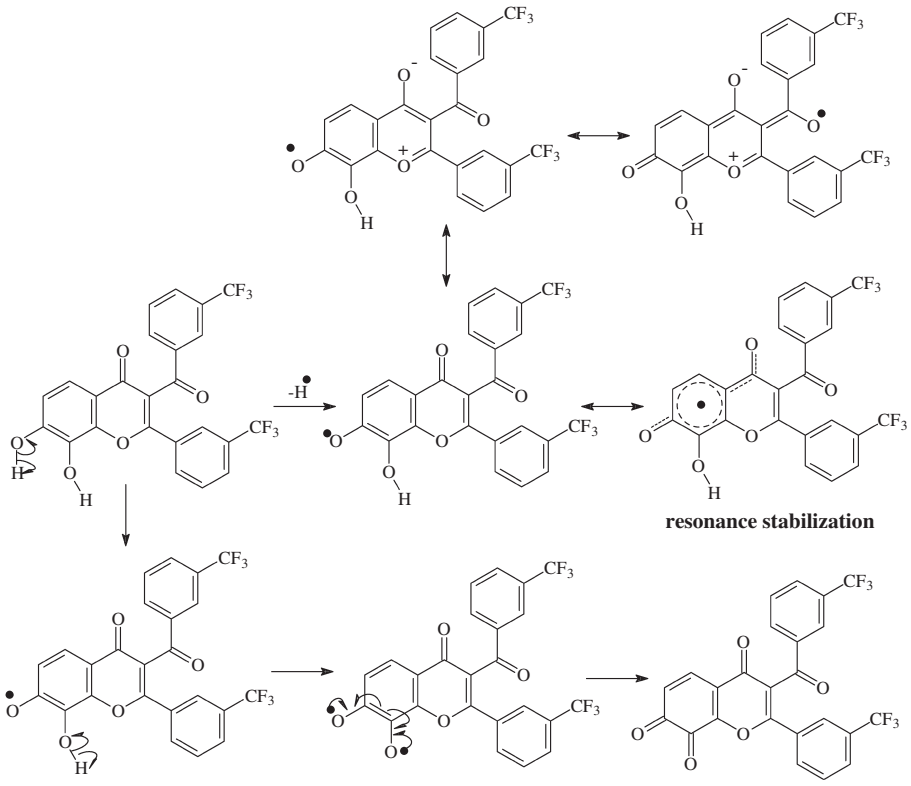

Fig. 3. Proposed mechanism of radical stabilization.

abstraction due to the radical stabilization (Fig. 3). The initial H atom abstraction occurs on the 7-OH group. The generated free radical is stabilized via the resonance of an unpaired electron. The semiquinone type radical is more reactive than the original phenol molecule, therefore second H atom liberation from the 8-OH group proceeds rapidly, leading to a quinone structure. These results support the SAR previously reported that effect of antioxidants on DPPH assay was thought to be due to their hydrogen donating ability [23,24].

These 3D-QSAR results provide structure–radical scavenging activity relationships: (i) an *ortho*-dihydroxy substitution (the presence of a catechol group) located at C-7 and C-8 of chromone nucleus is important for high activity, and (ii) the presence of hydrophobic substituents at C-2 and C-3 contribute to the higher activity. As shown in Table 1, compounds with 7,8-dihydroxy and C-2, C-3 substituents, i.e., chromones **32–37** exhibited strong activity (IC_{50} = 4.95–12.15 μM).

4. Conclusion

In this study, the ligand-based 3D-QSAR, CoMFA and CoMSIA have been successfully applied to a set of novel chromone series. Statistical parameters illustrate the established CoMFA and CoMSIA models are reliable. The contour maps provide significant relationships between structural features and radical scavenging activity. The catechol part (ring A) of chromones was essential feature which contributed to a greater stability of the formed aryloxy radicals via resonance stabilization. Moreover, the presence of hydrophobic groups at C-2 and C-3 were favored for enhanced activity. Consequently, the present study also gives the meaningful structural insights into possible modifications of chromone derivatives which could improve radical scavenging activity for the future work.

Acknowledgments

This research is supported by the Office of the Higher Education Commission and Mahidol University under the National Research Universities Initiative. The authors thank High Performance Computer Center (HPCC), National Electronics and Computer Technology Center (NECTEC) of Thailand for providing SYBYL version 8.1 facilities.

References

[1] B. Havsteen, Biochem. Pharmacol. 32 (1983) 1141–1148.
[2] J.B. Harborne, C.A. Williams, Phytochemistry 55 (2000) (1992) 481–504.
[3] M. Gabor, Prog. Clin. Biol. Res. 213 (1986) 471–480.
[4] V. Breinholt, A. Hossaini, G.W. Svendsen, C. Brouwer, E. Nielsen, Food Chem. Toxicol. 38 (2000) 555–564.
[5] C.G. Hu, K. Chen, Q. Shi, R.E. Kilkuskie, Y.C. Cheng, K.H. Lee, J. Nat. Prod. 57 (1994) 42–51.
[6] O.-V. Jesús, P.-L. Leonardo, J. Chem. Inf. Comput. Sci. 42 (2002) 1241–1246.
[7] W. Ren, Z. Qiao, H. Wang, L. Zhu, L. Zhang, Med. Res. Rev. 23 (2003) 519–534.
[8] S. Ramos, J. Nutr. Biochem. 18 (2007) 427–442.
[9] S. Teixeira, C. Siquet, C. Alves, I. Boal, P. Marques, F. Borges, J.L. Lima, S. Reis, Free Radic. Biol. Med. 39 (2005) 1099–1108.
[10] H.F. Ji, H.Y. Zhang, J. Mol. Struct. 767 (2006) 3–9.
[11] W. Bors, M. Saran, Free Radic. Res. Comm. 2 (1987) 289–294.
[12] N. Cotelle, Curr. Top. Med. Chem. 1 (2001) 569–590.
[13] A.S. Pannala, T.S. Chan, P.J. O'Brien, C.A. Rice-Evans, Biochem. Biophys. Res. Commun. 282 (2001) 1161–1168.
[14] B. Yang, A. Kotani, K. Arai, F. Kusu, Anal. Sci. 17 (2001) 599–604.
[15] J.W. Chen, Z.Q. Zhu, T.X. Hu, D.Y. Zhu, Acta Pharmacol. Sin. 23 (2002) 667–672.
[16] K.E. Heim, A.R. Tagliaferro, D.J. Bobilya, J. Nutr. Biochem. 13 (2002) 572–584.
[17] T. Yokozawa, C.P. Chen, E. Dong, T. Tanaka, G.I. Nonaka, I. Nishioka, Biochem. Pharmacol. 56 (1998) 213–222.
[18] N. Phosrithong, W. Samee, P. Nunthanavanit, J. Ungwitayatorn, Chem. Biol. Drug Des. 79 (2012) 981–989.
[19] A. Seyoum, K. Asres, E.-F. Kandeel, Phytochemistry 67 (2006) 2058–2070.
[20] R.D. Cramer, D.E. Patterson, J.D. Bunce, J. Am. Chem. Soc. 110 (1988) 5959–5967.
[21] G. Klebe, U. Abraham, T. Meitzner, J. Med. Chem. 37 (1994) 4310–4346.
[22] G. Klebe, U. Abraham, J. Comput-Aided Mol. Des. 13 (1999) 1–10.
[23] J.R. Soares, T.C.P. Dinis, A.P. Cunha, L.M. Ameida, Free Radic. Res. 26 (1997) 469–478.
[24] J. Baumann, G. Wurn, V. Bruchlausen, Naunyn Schmiedebergs. Arch. Pharmacol. 308 (1979) R27.